Report on the use of stability parameters and mesoscale modelling in short-term prediction

Badger, Jake; Giebel, Gregor; Larsén, Xiaoli Guo; Nielsen, T.S.; Nielsen, H. Aa.; Madsen, H.; Tøfting, J.

Publication date:
2007

Document Version
Publisher's PDF, also known as Version of record

Risø-R-Report

Report on the use of stability parameters and mesoscale modelling in short-term prediction

Jake Badger, Gregor Giebel, Xiaoli Guo Larsen, Torben Skov Nielsen, Henrik Aaborg Nielsen, Henrik Madsen, John Tøfting

Risø-R-1614(EN)

Risø National Laboratory
Technical University of Denmark
Roskilde, Denmark
June 2007

Author: Jake Badger, Gregor Giebel, Xiaoli Guo Larsen, Torben Skov Nielsen, Henrik Aaborg Nielsen, Henrik Madsen, John Tøfting
Title: Report on the use of stability parameters and mesoscale modelling in short-term prediction
Department: Wind Energy Department

Risø-R-1614(EN)
June 2007

Abstract (max. 2000 char.):

In this report investigations using atmospheric stability measures to improve wind speed predictions at wind farm sites are described. Various stability measures have been calculated based on numerical weather prediction model output. Their ability to improve the wind speed predictions is assessed at three locations. One of the locations is in complex terrain. Mesoscale modelling has been carried out using KAMM at this location. The characteristics of the measured winds are captured well by the mesoscale modelling. It can be seen that the atmospheric stability plays an important role in determining how the flow is influence by the terrain. A prediction system employing a look-up table approach based on wind class simulations is presented. The mesoscale modelling results produced by KAMM were validated using an alternative mesoscale model called WRF. A good agreement in the results of KAMM and WRF was found. It is shown that including a stability parameter in physical and/or statistical modelling can improve the wind speed predictions at a wind farm site. A concept for the inclusion of a stability measure in the WPPT prediction system is presented, and the testing of the concept is outlined.

ISSN 0106-2840
ISBN 978-87-550-3615-4

Contract no.:

Group's own reg. no.:
(Føniks PSP-element)

Sponsorship:

Cover :

Pages:
Tables:
References:

Information Service Department
Risø National Laboratory
Technical University of Denmark
P.O.Box 49
DK-4000 Roskilde
Denmark
Telephone +45 46774004
bibl@risoe.dk
Fax +45 46774013
www.risoe.dk

Report on the use of stability parameters and mesoscale modelling in short-term prediction

PSO (FU 4101)
Intelligent Prognosis Systems for Wind Power

Jake Badger[1], Gregor Giebel[1], Xiaoli Guo Larsen[1], Torben Skov Nielsen[2], Henrik Aaborg Nielsen[2], Henrik Madsen[2], John Tøfting[3]

[1] Risø National Laboratory/Technical University of Denmark, Wind Energy Department, DK-4000 Roskilde
[2] Technical University of Denmark, Informatics and Mathematical Modelling, DK-2800 Lyngby
[3] Elsam Kraft A/S, DK-7000 Fredericia DK-2800 Lyngby

June 26, 2007

Contents

1 Summary

In this report investigations using atmospheric stability measures to improve wind speed predictions at wind farm sites are described. Various stability measures have been calculated based on numerical weather prediction model output. Their ability to improve the wind speed predictions is assessed at three locations. One of the locations is in complex terrain. Mesoscale modelling has been carried out using KAMM at this location. The characteristics of the measured winds are captured well by the mesoscale modelling. It can be seen that the atmospheric stability plays an important role in determining how the flow is influence by the terrain. A prediction system employing a look-up table approach based on wind class simulations is presented. The mesoscale modelling results produced by KAMM were validated using an alternative mesoscale model called WRF. A good agreement in the results of KAMM and WRF was found. It is shown that including a stability parameter in physical and/or statistical modelling can improve the wind speed predictions at a wind farm site. A concept for the inclusion of a stability measure in the WPPT prediction system is presented, and the testing of the concept is outlined.

2 Introduction

Within the EU-funded Anemos project (ENK5-CT-2002-00665) physical modelling approaches to improving wind power predictions were investigated, Giebel et al. (2005). The Karlsruhe Atmospheric Mesoscale Model (KAMM) was used to construct a look-up table to provide appropriate adjustments of the *numerical weather prediction* (NWP) wind speed and direction to give *wind farm* wind speed and direction. However, in that study it was found that using only limited information about the state of the atmosphere in depth, limited the scope of using KAMM mesoscale modelling for short term prediction. Those limitations have been removed in the study described here by using much more information about the vertical variation of wind and temperature in the atmosphere.

The stability of the atmosphere is important in determining the behaviour of winds near the surface or over complex terrain. The important concepts and measures of boundary layer and deeper atmospheric stability are described in the following subsections.

2.1 Potential temperature and stability

Atmospheric pressure decreases with height, such that if an air parcel is lifted its temperature will decrease as the air parcel expands adiabatically. In a neutrally stratified atmosphere the environmental air temperature changes exactly as the air parcel temperature changes as it is lifted, such that the air parcel and the environmental air at a new

height have the same temperature. Thus no density difference exists, and no buoyancy force is generated.

Potential temperature, θ, is defined by

$$\theta = T\left(\frac{p_0}{p}\right)^{\frac{R}{C_p}} \ , \tag{1}$$

where T and p are the temperature and pressure of the air of interest, p_0 is the standard pressure, usually taken as 1000 hPa, R is the gas constant for air (287 $JK^{-1}kg^{-1}$ for dry air), and C_p is the specific heat capacity of air at constant pressure (1004 $JK^{-1}kg^{-1}$). The potential temperature gives the temperature air would have if brought to standard pressure p_0 adiabatically.

- For stably stratified air, the partial derivative of θ with respect to height, z, is positive, i.e.
$$\frac{\partial\theta}{\partial z} > 0 \ , \tag{2}$$
meaning that a vertically displaced air parcel will experience a restoring buoyancy force, so as to accelerate the the air parcel back to its original position.

- For unstable air
$$\frac{\partial\theta}{\partial z} < 0 \ , \tag{3}$$
meaning that a vertically displaced air parcel will experience a buoyancy force accelerating it further away from its original position.

- For neutrally stratified air
$$\frac{\partial\theta}{\partial z} = 0 \ , \tag{4}$$
meaning that a vertically displaced air parcel will experience no buoyancy force.

2.2 Surface layer profile

For a neutrally stratified surface layer, the wind speed profile is well modelled by the logarithmic profile, where the wind speed, u, at height, z, can expressed as

$$u(z) = \frac{u_*}{\kappa}\log\left(\frac{z}{z_0}\right) \ , \tag{5}$$

where u_* is the friction velocity, related to the surface stress, τ, via $\|\tau\| = \rho u_*^2$, where ρ is density, κ is the von Karmen constant (here given the value 0.4, see Hogström (1988)) and z_0 is the aerodynamic roughness length.

In the atmospheric boundary layer, the stability is mainly governed by the heating or cooling of the surface. On a clear night for example the ground surface quickly cools, thereby cooling the air in contact with it. This tends to result in a stable surface layer. Conversely, during a sunny day, the ground surface will warm, thereby warming the air in contact with it, resulting in an unstable surface layer.

In non-neutral conditions a correction is added to logarithmic profile based on Monin-Obukhov similarity theory, such that

$$u(z) = \frac{u_*}{\kappa}\left(\log\frac{z}{z_0} + \psi\left(\frac{z}{L}\right)\right) \ , \tag{6}$$

where ψ is a function of z/L; L is the Monin-Obukhov length (Dyer (1974)). The Monin-Obukhov length is given by

$$L = \frac{T_0 c_p u_*^3}{\kappa g H_0} \ , \tag{7}$$

where H_0 is the surface heat flux towards the ground, g is the acceleration due to gravity, and T_0 is the surface temperature. When heat is being transported upward, away from for example a hot ground surface, then $H_0 < 0$ and unstable conditions prevail with $L < 0$. When heat is being transported downward, towards for example a cold ground surface, then $H_0 > 0$ and stable conditions prevail with $L > 0$. The functions for ψ have been found empirically and depend on the stability, Jensen et al. (1984).

For unstable conditions ($L < 0$),

$$\psi = (1 - 16\frac{z}{L})^{\frac{1}{4}} - 1 \ . \tag{8}$$

For stable conditions ($L > 0$),

$$\psi = -4.7\frac{z}{L} \ , \tag{9}$$

In neutrally stratified conditions the heat flux is zero and $L = \infty$ and $\psi(\frac{z}{L}) = 0$, such that (6) becomes the same as (5).

Figure 1 shows three wind profiles based on the Monin-Obukhov similarity theory profiles

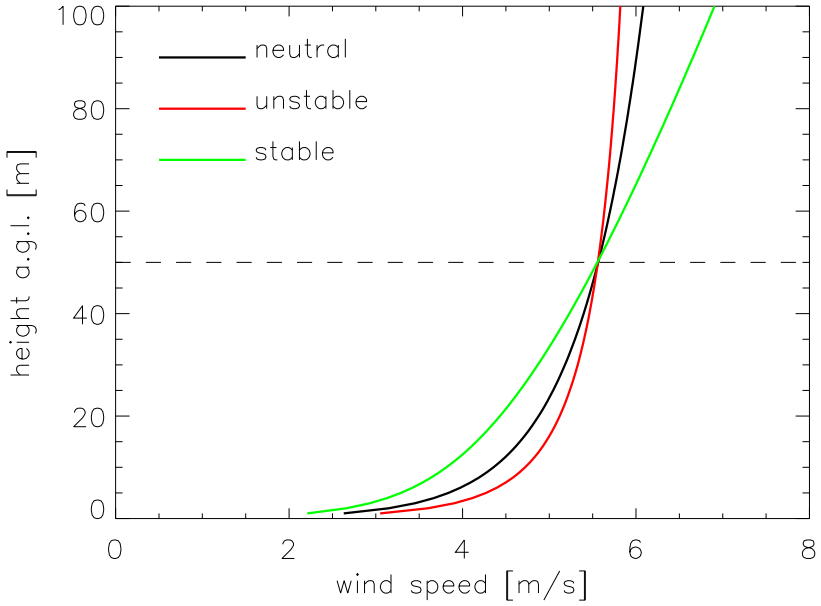

Figure 1: Plot showing the wind profiles for different stability conditions, based on Monin-Obukhov similarity theory and Monin-Obukhov length, L; for neutral conditions $L = 0$, for unstable conditions $L < 0$, and for stable conditions $L > 0$.

described above for stable, neutral and unstable conditions. The values of u_* and L have been adjusted to get the same wind speed at 50 m above ground level (a.g.l.).

The shape of the profile is markedly different for different stability conditions. Therefore it may be expected that without taking into account of stability conditions an error will be introduced when extrapolating wind speed from one height to another height.

2.3 Flow over terrain

The way in which wind flow is modified by terrain is related to the stability of the atmosphere. As examples, terrain features such as a valley or a pass can act to channel the flow, or a high ridge may act to block flow. The degree to which the terrain features act as channels or obstacle to the wind depends on how much the flow is able to be displaced vertically. If the vertical displacement of the air is uninhibited then the flow is likely to pass over the terrain without much deviation due to the terrain features. However, if vertical displacement of the air is inhibited then the flow is likely to channelled and blocked by terrain features. In each case the appropriate scale for the vertical displacement is the vertical scale of the terrain. In the case of a stably stratified atmosphere, in order for the vertical displacement of the air to be achieved energy is required, and this can come from the kinetic energy in the flow.

The Froude number, Fr, is useful in determining how wind will be modified by terrain,

Kaimal and Finnigan (1994). It is sometimes stated as the ratio of inertial force to the reduced gravity force accounting for buoyancy effects. When $Fr > 1$ the flow is able to pass over the terrain obstacle. When $Fr < 1$ the flow is unable to pass over the obstacle, resulting in the flow being diverted around the obstacle, if possible, or simply being blocked. The Froude number has many applications and various definitions, here it is defined as

$$Fr = \frac{u}{hN} \ , \tag{10}$$

where u is the wind speed, h is the obstacle height, N is the Brunt-Väisälä frequency,

$$N = \sqrt{\frac{g}{\theta_0}\frac{\partial\theta}{\partial z}} \ . \tag{11}$$

N is a measure of the stability of the air. For higher values of N the restoring buoyancy force felt by a vertically displaced parcel of air is larger. Thus more work has to be done in order to displace the air vertically. A typical tropospheric value of N is $1.2 \times 10^{-2} s^{-1}$.

Considering a hill with a height, h, equal to 500 m, a wind speed, u, equal to 10 ms^{-1}, and $N = 1.2 \times 10^{-2} s^{-1}$, gives $Fr \simeq 1.7$. Therefore the flow is able to pass over the hill in this case.

However if the wind speed is reduced to below 6 ms^{-1}, or the hill is extended to over $\simeq$ 850 m high, or the static stability is increased to over $2 \times 10^{-2} s^{-1}$, then the flow will not easily pass over the hill.

Figure 2 shows a schematic diagram for the flow over or around a hill depending on the Froude number.

3 Method

The methods within this article can be broken down into three areas:

- Statistical investigation of the importance of a stability parameter
  The importance of stability information is tested by a simple linear regression method. The tests are carried out for three meteorological mast locations. Two of these masts are located at wind farm sites, one in simple terrain and one in complex terrain.

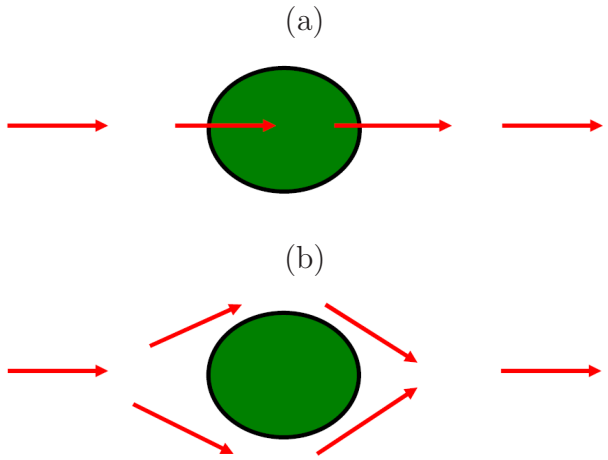

Figure 2: Diagram showing plan view of (a) flow over a hill when $Fr > 1$ and (b) flow around a hill when $Fr < 1$.

- Mesoscale model investigation of the region wind flow dependence on stability
  The Karlsruhe Atmospheric Mesoscale Model (KAMM, Adrian and Fiedler (1991)) is used to identify how the flow is modified by topography for a set of representative wind conditions. These representative sets of wind conditions include different stability situations as well as wind speed and direction. The mesoscale modelling results are then used to define a correction matrix for use in a wind farm wind speed prediction system. To validate the results the mesoscale model WRF is used in place of KAMM a comparison of the results is made.

- Application of a stability parameter
  The results of the linear regression method for the complex terrain wind farm could be used in a preprocessor setup along side an operation wind power prediction system. The flow structure for doing this kind of application is proposed in section 9.

3.1 Global Forecast System (GFS)

In all of the investigations in this report the numerical weather prediction model output used comes from the Global Forecasting System (GFS) model, operated by the National Center for Environmental Prediction (NCEP).

The model is a global spectral model with four forecast cycles per day at 0Z, 6Z, 12Z, 18Z. The maximum forecast horizon or leadtime is 384 hours (16 days). The resolution of the model is T382 out to a leadtime of 180 hours and T190 from 180 hours to 384 hours. For spectral models the state of the atmosphere is described using harmonic basis functions in the latitude and longitude direction. A resolution termed T382 means that highest total wavenumber is 382, giving a resolution of approximately 50 km. The letter 'T' refers to the triangular truncation that is used, describing how the longitudinal and latitudinal

wavenumbers are configured. Another truncation method is rhomboidal referred to with the letter 'R'. The model uses 64 vertical levels.

Output from the model is available freely via the internet. Everyday since August 2005 a LINUX computer at the Wind Energy Department downloads the following data from the 0Z forecast cycle for Europe out to a leadtime of 180 hours (7.5 days):

westerly and southerly wind velocity components (u,v) at 10 m, temperature at 2 m, surface temperature, and temperature and geopotential height at 1000, 850, 700, 500, 250 hPa. From these data the following 'deep profile' quantities are calculated:

- wind speed and direction at 10 m (U_{10}, D_{10}).
- geostrophic wind speed and direction at 1000, 850, 700, 500, 250 hPa (U^g_{1000}, U^g_{850}, U^g_{700}, U^g_{500}, U^g_{250}, D^g_{1000}, D^g_{850}, D^g_{700}, D^g_{500}, D^g_{250}).
- potential temperature at 1000, 850, 700, 500, 250 hPa (θ_{1000}, θ_{850}, θ_{700}, θ_{500}, θ_{250}).

For Denmark the following supplementary data is downloaded: mean wind westerly and southerly velocity components (u,v) and temperature for layers defined by the following pressure intervals *above* the surface: 30 - 0, 60 - 30, 90 - 60, 120 - 90, 150 - 120, 180 - 150 hPa. From these data the following 'shallow profile' quantities are calculated:

- mean wind speed and direction for the layers 30 - 0, 60 - 30, 90 - 60 , 120 - 90, 150 - 120, 180 - 150 hPa (U_{30-0}, U_{60-30}, U_{90-60},U_{120-90}, $U_{150-120}$, $U_{180-150}$, D_{30-0}, D_{60-30}, D_{90-60}, D_{120-90}, $D_{150-120}$, $D_{180-150}$).
- mean potential temperature for the layers 30 - 0, 60 - 30, 90 - 60 , 120 - 90, 150 - 120, 180 - 150 hPa (θ_{30-0}, θ_{60-30}, θ_{90-60}, θ_{120-90}, $\theta_{150-120}$, $\theta_{180-150}$).

For the calculation of the potential temperature, the mean pressure for each layer is used. The approximate mean height for each layer is 130, 380, 370, 890, 1150, 1400 m. The exact heights will depend on the temperature of the layers, and thus change depending on atmospheric conditions.

These meteorological quantities are used in a range of stability parameters, detailed in the following section.

3.2 Stability parameters

The Brunt-Väisälä frequency, N, has already been described in section 2 as a stability parameter. Other parameters were also used, although these are not all strictly stability parameters as N is. They do however give further information about the wind profile. The parameters tested were:

$$G_\theta = \frac{\partial \theta}{\partial z} \tag{12}$$

$$G_u = \frac{\partial u}{\partial z} \tag{13}$$

$$U_z = u \tag{14}$$

$$N^2 = \frac{g}{\theta_0}\frac{\partial \theta}{\partial z} \tag{15}$$

$$Fr^2 = (\frac{u}{hN})^2 \tag{16}$$

These were discretized using the NWP data as

$$G_\theta = \frac{\theta_h - \theta_l}{z_h - z_l} \tag{17}$$

$$G_u = \frac{u_h - u_l}{z_h - z_l} \tag{18}$$

$$U_z = u_h \tag{19}$$

$$N^2 = \frac{2g(\theta_h - \theta_l)}{(\theta_h + \theta_l)(z_h - z_l)} \tag{20}$$

$$Fr^2 = \frac{u_l^2(\theta_h + \theta_l)}{g(\theta_h - \theta_l)(z_h - z_l)} \tag{21}$$

The subscripts indicate the level at which a quantity is taken for the calculation, thus θ_h and θ_l refer to θ for higher and lower levels respectively. Different levels for θ, u and z were tested.

The stability parameters were calculated using the 'deep profile' and the 'shallow profile' data.

3.3 Linear regression performance test

There are various ways in which the NWP wind speed data can be used to make a prediction for an observed wind speed. The simplest is to use the NWP wind speed directly, for example using U_{10} for the nearest NWP model grid point. It is also possible to calculate the wind speed at a different height based on U_{10} for example by using the logarithmic profile (5).

The error for these kinds of predictions very often contains a significant systematic error, for example a bias, that can be reduced by *Model Output Statistics* (MOS). The MOS model used in this study was

$$U_{pred} = A + BU_{NWP} \ . \tag{22}$$

Where A and B are found by fitting a linear regression using a training period of the concurrent NWP and observed winds time series, where A and B can be functions of the wind direction, D_{NWP}. This allows the influence of local features, such as changes in surface roughness that may depend on direction, to be accounted for. This is usually done by binning direction into twelve 30° wide direction sectors. A and B can also be functions of forecast horizon.

Next the usual MOS can be extended by putting the stability parameter into the linear regression

$$U_{pred} = A + BU_{NWP} + CS_{NWP} \ , \tag{23}$$

where S_{NWP} represents a chosen stability parameter from the NWP data. Again C, like A and B, can be a function of wind direction.

It is of interest to see in which cases an improvement in the prediction skill can be achieved when using the linear regression *with* the stability parameter compared to the linear regression *without* the stability parameter. The prediction skills were compared by calculating mean error (ME) and mean absolute error (MAE),

$$ME = \frac{\sum_{i=1}^{N} \left(U_{obs}^{i} - U_{pred}^{i}\right)}{N} \tag{24}$$

$$MAE = \frac{\sum_{i=1}^{N} |U_{obs}^{i} - U_{pred}^{i}|}{N} \ , \tag{25}$$

where N here is the number of observations. The first step was to use the full time series of forecasts and observations as both the training period and the testing period.

The second step is to split the time series into two halves, one for training and other for testing. The split can be done in a number of ways. In this study the split was done in two ways. One way is to split the time series into two continuous periods half way through the time series. The other way is to take half of the time series data randomly for the training, then the remaining half of the data is used for the testing. Any robust improvement when using the stability parameter is shown by a consistent improvement when using the out-of-sample testing data.

4 Wind speed prediction for the Risø mast

Data from the meteorological mast at Risø National Laboratory for the six month period 01/09/2005 - 28/02/2006 has been used with the GFS data over the same period to test the various stability parameters.

The mast is 118 m high and equipped with anemometers at various heights. The anemometer at 76 m a.g.l. was selected because this represents a typical hub height of a modern wind turbine.

Table 1 gives a summary of the stability parameters' skill for the prediction system based on training data randomly sampled from the time series data. Half the data is used for the training. The testing data is the remaining time series data not used for the training.

U_{NWP}	U_{30-0}		U_{10}		U^g_{1000}		U^g_{850}	
MOS MAE	1.26		1.37		2.11		2.13	
S	MAE	Δ%	MAE	Δ%	MAE	Δ%	MAE	Δ%
shallow profile stability measures								
G_θ	1.25	-0.81	1.34	-2.39	2.10	-0.60	2.14	-0.18
G_u	NI		1.32	-3.56	1.67	-20.9	1.68	-21.3
u_z	NI		1.29	-5.62	1.31	-38.0	1.31	-38.1
N^2	1.25	-0.73	1.34	-2.22	2.09	-0.51	NI	
Fr^2	NI		1.37	-0.16	NI		NI	
deep profile stability measures								
G_θ	NI		NI		2.08	-1.25	2.13	-0.60
G_u	NI		NI		2.09	-0.68	2.09	-2.08
N^2	NI		NI		2.09	-1.05	2.12	-0.49
Fr^2	NI		NI		NI		2.12	-0.90

Table 1: The performance in terms of mean error (ME) and mean absolute error (MAE) in ms^{-1} of the different NWP stability parameters for Risø wind speed predictions. NI indicates that there was no improvement on performance when using the stability parameter. The errors are based on the 0 hour leadtime forecasts.

First it should be noted that the predictions based on MOS alone, i.e. without using a stability parameter, are best when using U_{30-0} as NWP wind input, with a mean absolute error of 1.26 ms^{-1}. This is better than using the U_{10} as NWP wind input. Not unexpectedly the geostrophic wind at 1000hPa and 850hPa as NWP wind input gives a poorer performance.

First the use of the shallow profile stability measures in the linear regression is considered. The best improvement on the MOS performance for the U_{30-0} NWP wind input is achieved using the G_θ measure which is evaluated using θ_{30-0} and θ_{60-30}. However the relative improvement is rather small at only -0.81%. Using N^2 also gives a small relative improvement of the performance (-0.73%). All of the other stability measures do not give an improvement.

The best improvement on the MOS performance for the U_{10} NWP wind input is achieved using the u_z measure, evaluated using U_{60-30}. This gives a relative improvement of -5.62%. This can be understood in terms of adding a better wind speed forecast relative to the U_{10} forecast to the system. In this way the mean absolute error is brought down to a value close to the mean absolute error using the U_{30-0} NWP wind alone with MOS.

Except for the Fr^2 stability measure, the other shallow profile measures give an improvement of between -2.22% and -3.56% when used with the U_{10} NWP wind input. However, the mean absolute error never goes below the best U_{30-0} prediction.

When using the geostrophic winds, U^g_{1000} and U^g_{850}, as NWP wind input, large improvements in performance are achieved when using the G_u and u_z stability measures, approximately 20% and 40% respectively. The large improvement when using u_z can be understood in terms of simply adding a better wind forecast to the system, in the same way that the U_{10} forecast was improved. The improvement achieved using the G_u measure may be due to there being a correlation between stronger surface winds and higher wind shear.

Next the use of the deep profile stability measures is considered. For the U_{30-0} and U_{10} NWP wind input no improvement of the performance is achieved for any of the stability measures. For the geostrophic NWP wind input U^g_{1000} a small improvement (-1.25%) is achieved using the G_θ stability measure. For the U^g_{850} NWP wind input, the largest performance improvement is achieved by using G_u measure. This gives a performance equal to using the U^g_{1000} as input and G_u as stability measure. This can be understood by considering that a linear combination of U^g_{850} and G_u can give exactly the result as a linear combination of the U^g_{1000} and G_u, since $G_u = (U^g_{850} - U^g_{1000})/\Delta z$.

5 Wind speed prediction for the Alaiz mast

Data from a 55 m a.g.l anemometer mounted on one of the Alaiz wind farm's meteorological masts for the period 01/07/2004 - 31/05/2005 has been used with the GFS data covering the same period to test the various stability parameters. The GFS data was provided by CENER, Spain, because the observation data period is before the date GFS forecasts downloading began at Risø. The GFS data available from CENER covers nearly the same meteorological fields as those downloaded at Risø. However only the closest to surface 30-0 hPa pressure layer is available. On the other hand more pressure level data was available, allowing U, D and θ to be determined on 1000, 850, 700, 500, 250 hPa levels. This was essential for the modelling done in section 7.

Table 2 gives a summary of the stability parameters' performance for the prediction system based on training data randomly sampled from the time series data. Half the data is used for the training. The testing data is the remaining time series data not used for the training.

U_{NWP}	U_{30-0}		U_{10}	
MOS MAE	2.98		3.19	
S	MAE	Δ%	MAE	Δ%
shallow profile stability measures				
G_θ	2.93	-1.66	3.04	-4.59
G_u	2.95	-0.99	2.95	-7.37
u_z	2.95	-0.99	2.95	-7.37
N^2	NI		3.12	-2.10
Fr^2	NI		NI	
deep profile stability measures				
G_θ	2.51	-15.0	2.58	-19.0
G_u	NI		3.15	-1.07
u_z	2.97	-0.13	3.08	-3.16
N^2	2.48	-16.6	2.56	-19.88
Fr^2	NI		3.08	-3.36

Table 2: The performance in terms of mean error (ME) and mean absolute error (MAE) in $\mathrm{ms}^{-1}$of the different NWP stability parameters for Alaiz wind speed predictions. NI indicates that there was no improvement on performance when using the stability parameter. The errors are based on forecast leadtimes in the range 0 to 48 hours.

The mean absolute error from using MOS alone using U_{30-0} and U_{10} gives a mean absolute error of 2.98 and 3.19 ms^{-1} respectively. Compared to the performance using MOS alone for the Risø mast data it can be seen that the performance for the Alaiz wind prediction is much less accurate.

When using the shallow profile stability measures, the best performance giving a mean

absolute error of 2.93 ms^{-1} is achieved by using the U_{30-0} with G_θ, although this combination gives only a relative improvement of mean absolute error of -1.66%. Using the U_{10} with additional wind speed, u_z or wind shear data, G_u improved the performance by -7.37%. In this case $u_z = (U_{10} + U_{30-0})/2$ and $G_u = (U_{10} - U_{30-0})/\Delta z$. Linear combinations of U_{10} with G_z, U_{10} with u_z, U_{30-0} with G_z, and U_{30-0} with u_z, can give the same result. Therefore the mean absolute error for these combinations is the same at 2.95 ms^{-1}.

The most dramatic improvements in prediction performance are seen when using the deep profile stability measures. Using G_θ or N^2 stability measures gives a relative change of the mean absolute error of approximately -15% and -20%, for U_{30-0} and U_{10} wind inputs respectively. Using U_{30-0} with N^2 gives a mean absolute error of 2.48 ms^{-1}which is the minimum mean absolute error obtained. It was found that the improvements in mean absolute error was optimal when calculating G_θ and N^2 using θ_{1000} and θ_{700}, rather than using other combinations of pressure levels. This is interesting because it represents a vertical scale of approximately 3000 m.

It can be seen that it is the information about the thermal stratification that is most useful in reducing the mean absolute error of wind speed predictions. Stability measures containing wind speed or wind speed shear have a smaller impact on the performance in contrast.

A physical basis of these result emerges from the result of section 7.

6 Wind speed prediction for the Klim mast

Data from two anemometers mounted at 46 m above ground level on two meteorological masts at the Klim wind farm, Denmark, for the six month period 01/12/2005 - 31/03/2006 have been used with the GFS data covering the same period to test the various stability parameters.

Using MOS alone gives wind speed predictions with a mean absolute error of 1.2 m/s. It was not possible to make significant improvements of the wind speed prediction using any of the stability measures.

The reasons for this may be related to the anemometer heights or connected to the NWP stability measures being inaccurate for that region, possibly due to proximity and complexity of the coastline. Alternatively it could be related to the possibility that the GFS model performs very well without any need to have any stability corrections, i.e. the stability corrections are superfluous. It is difficult to know the precise grounds for the lack of improvement, however it was decided that time and effort should be dedicated to investigating the Alaiz case where a strong improvement in performance was found.

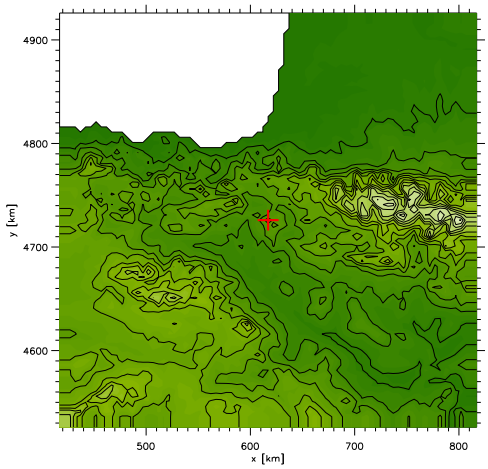

Figure 3: A map showing surface elevation contours, the location of the Alaiz wind farm (red cross) and the KAMM modelling domain. The coordinate system is UTM zone 30. The contour interval is 200 m. The domain is 400 x 400 km in size and is represented by 81 x 81 grid points, giving a resolution of 5 km.

7 Mesoscale modelling for Aliaz

The Alaiz wind farm is a challenging wind farm to provide accurate wind and power forecasts for and has been the subject of numerous investigations, some of which have been conducted as part of the EU-funded ANEMOS project.

The wind farm is located on an approximately 1000-m high mountain, located between regions of even higher elevated terrain. Figure 3 shows the elevation map of the area. Surface elevation data and surface roughness data were derived from the GTOPO30 and Global Land Cover Classification respectively. Both of these datasets come from the United States Geological Survey.

Figure 3 is also the modelling domain used in Karlsruhe Atmospheric Mesoscale Model (KAMM, Adrian and Fiedler (1991)). It was found that the size of the domain needs to be at least 400 x 400 km in order to include the important topographical features influencing the flow in the region of the Alaiz wind farm.

7.1 Region wind flow around the Alaiz wind farm

Idealized KAMM studies have been performed using sets of wind profiles representing different wind directions and different atmospheric stabilities. Four different geostrophic wind speed profiles (5, 10, 15, 20 m/s) and three different stabilities, neutral, typical (near neutral) and stable, were investigated.

The geostrophic wind and temperature profiles were defined at 0, 1500, 3000, 5500 m above sea level. The geostrophic wind speeds forcing the model were constant with height. For the stable and typical stability cases the temperature profiles were evaluated using NCEP/NCAR reanalysis data.

Figure 4 summarizes the results for five sets of the idealized KAMM simulations. The thick rectangles show the forcing directions, e.g. the sector centred on 30° is red. For a given large-scale forcing the simulated winds at 50 m for five locations neighbouring the wind farm are show by lines of the same colour. The direction on the diagram indicates the direction where the wind comes from and the length indicates the wind speed speed-up. The dotted-line circle represents a speed-up of 1, meaning that the wind speed at 50 m is the same as the geostrophic forcing. A speed-up above 1 indicates a wind faster than the forcing wind speed and below 1 indicates a wind slower than the wind forcing.

Looking at Fig. 4(c) first, the set using 10 ms^{-1} geostrophic winds and typical stability, it is possible to see that the wind directions at the wind farm site tend to be concentrated into the northern and south-eastern sectors, whatever the forcing wind direction is. Examining next Fig. 4(e), the set using 5 ms^{-1} geostrophic winds and typical stability, it is possible to see that the direction concentration effect is slightly enhanced and that there is a greater degree of speed-up of the winds. A similar behaviour is seen when examining Fig. 4(b), the set using 10 ms^{-1} winds and stable stratification. Figure 4(a) shows the set of simulations using 20 ms^{-1} winds and typical stratification. Here it is possible to see a reduction in the direction concentrating effect of the winds at the wind farm, and a reduced speed-up effect. Figure 4(d) shows the set using 10 ms^{-1} winds and neutral stratification. More so than in the case of Fig. 4(a) it shows a further reduction in the direction concentrating effect and speed-up.

The separate plots in Fig. 4 have been arranged such that when moving from left to right of the figure the simulation sets have increasing Froude number. Also when moving from bottom to top of the figure the Froude number increases. It can been seen then that the Froude number using the large scale winds and deep profile stratification characterizes the behaviour of the modelled winds at the Alaiz wind farm site.

To summarize, a lower Froude flows number tends to give more concentrated wind directions and a higher degree of speed-up compared to higher Froude number flows.

Figure 5 shows the wind a 50 m a.g.l. for the 10 ms^{-1} 240° forcings using the three different deep profile stabilities. The plots show the reduced surface winds in the lower lying Navarra valley region for the typical stratification (b) and neutral (c) cases, compared to the stably stratified case (a).

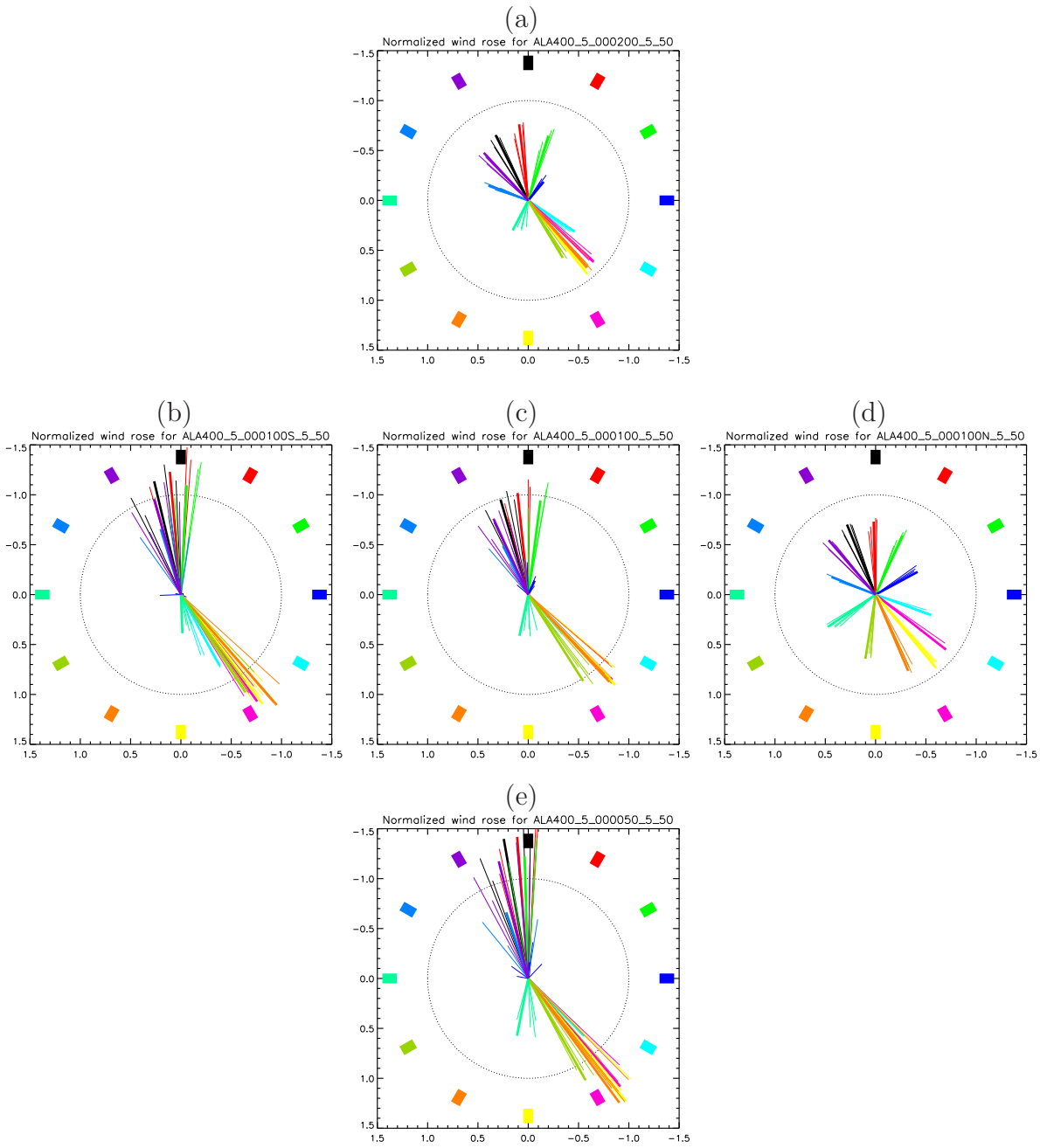

Figure 4: Diagrams showing the mesoscale effects on the geostrophic wind forcings for five sets of KAMM simulation using different wind speed and thermal stratifications, (a) 20 ms^{-1} and typical stability, (b) 10 ms^{-1} and stable conditions, (c) 10 ms^{-1} and typical stability, (d) 10 ms^{-1} and neutral conditions, (e) 5 ms^{-1} and typical stability. Each set is made up of twelve simulations using different wind direction indicated by colour. Please refer to the main text for an explanation of the figures.

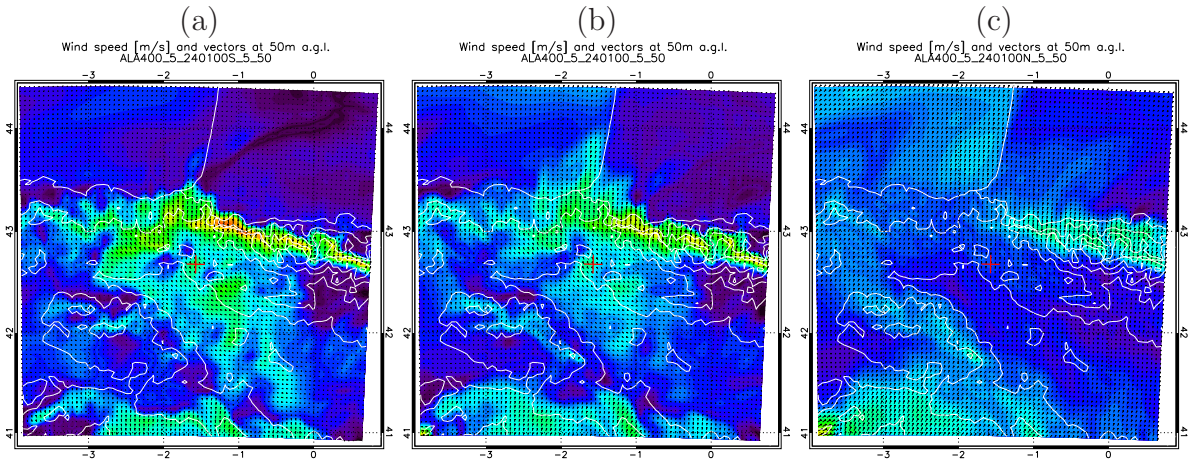

Figure 5: Maps showing the wind field at 50 m a.g.l. around the Alaiz wind farm, marked with the red cross, for 3 different stability conditions. The wind forcing is 10 ms^{-1} from 240°. Map (a) is for stably stratified conditions, (b) is for typical stability conditions, and (c) is for neutrally stratified conditions.

7.2 The wind class system and a look-up table approach to short-term wind speed prediction

The Karlsruhe Atmospheric Mesoscale Model (KAMM, Adrian and Fiedler (1991)), is used at Risø in conjunction with the WAsP software to create numerical wind atlases for regions (Frank and Landberg (1997)). The method employs a procedure which creates a set of wind classes that represent the range of large scale wind forcings and atmospheric stability that occur in the region of interest over the long-term. Simulations utilizing these wind classes are used to construct a modelled wind climate via statistical-dynamical downscaling (Frey-Buness et al. (1995)).

This wind class procedure needs input of the geostrophic wind and temperature at different heights in the atmosphere. In this study the data has come from both the NCEP/NCAR reanalysis and from the GFS forecast data provided by CENER.

The NCEP/NCAR reanalysis data was used to create a set of wind classes for the year 2001. The geostrophic wind speed and direction derived from the NCEP/NCAR reanalysis data for the complete year 2001 at nearest grid point and the derived wind classes are shown in Fig. 6.

These 108 wind classes were used as forcing conditions in KAMM simulations. The modelled wind speed at 50 m a.g.l. for the wind farm site is shown in Fig 7(a). Figure 7(b) shows the observed distribution of wind speed and direction at 55 m a.g.l. It can be seen that the direction concentrating effect of the topography at the wind farm site is evident in both the KAMM simulations and the observations. The rarity of wind direction measurements in the range 50-120° is mirrored by the near absence of modelled winds in

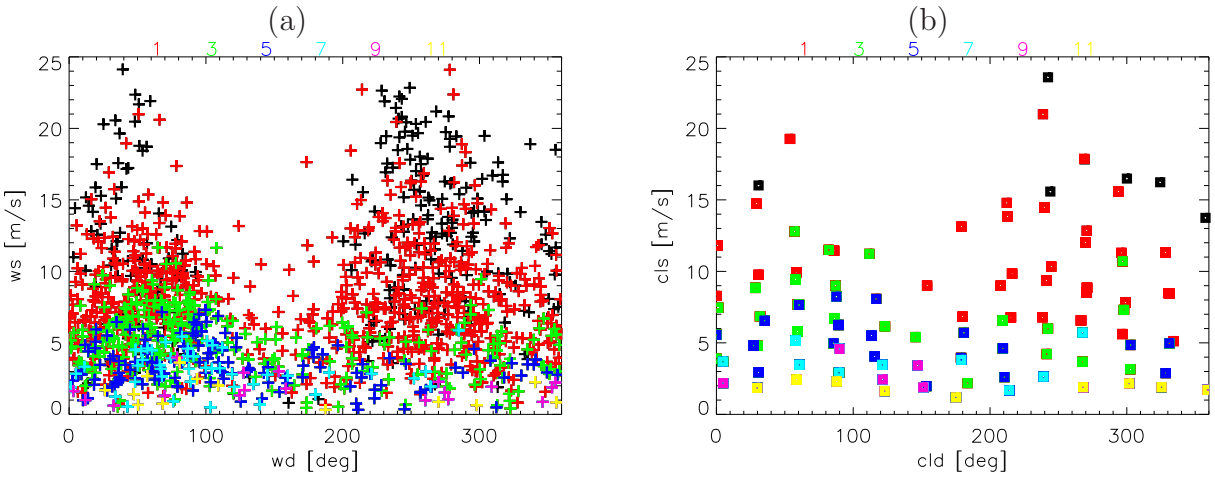

Figure 6: (a) The geostrophic wind and direction at 1°W 43°N at 0 m a.g.l. from the NCEP/NCAR four times daily reanalysis data for 2001, and (b) the geostrophic wind and direction for the 108 wind classes that have been calculated to represent the data in (a). The colours of the plotted points indicate the values of $1/Fr^2$, the colour key is provide by the colour of the values above the plots.

that range; just one wind class gives winds within that range. The presence of only low wind speeds in the direction range 200-300°is also captured.

In order to use the wind class system in a short-term prediction the preparatory tasks are as follow:

- generation of wind classes representing all large scale wind forcings and atmospheric stabilities occurring in the region of the wind farm.
- simulation using KAMM of the mesoscale winds in the region of the wind farm, generated by the regional scale topography using the generated wind classes as forcings.
- creation of a look-up table from the mesoscale results that associates a given large-scale forcing and stability with the modelled wind speed and direction at the wind farm site.

In order to apply the wind class system and the KAMM simulations, for each new GFS forecast cycle the following procedure is carried out:

- determine which wind class best matches the large scale wind forcing and atmospheric stability for each forecast leadtime.
- for each forecast leadtime, check the look-up table to find the modelled wind farm wind speed and direction using the appropriate wind class.

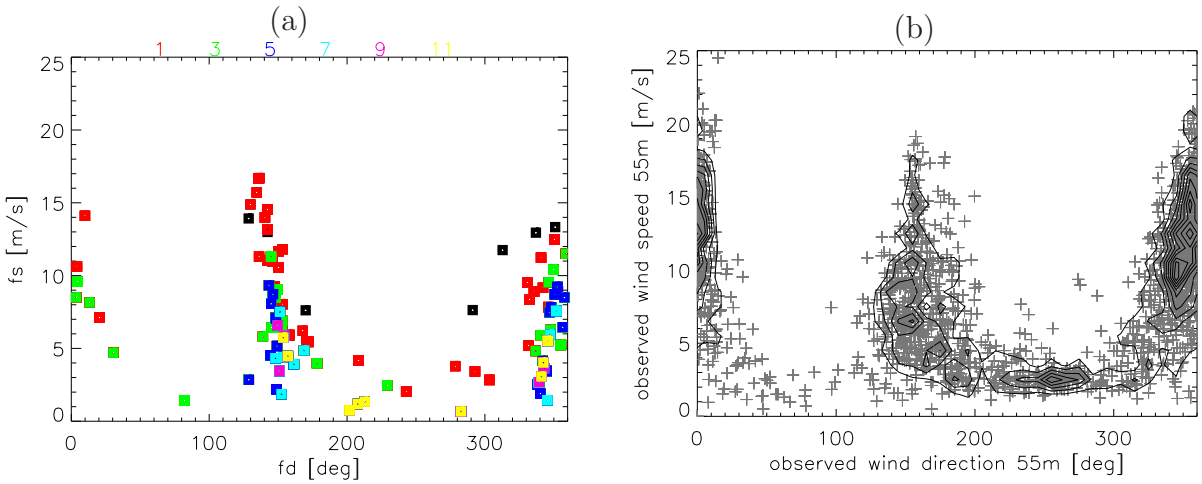

Figure 7: (a) The KAMM modelled wind speed and direction at 50 m a.g.l. at the wind farm site resulting from the simulations using the wind classes shown in Fig 6(b), and (b) the observed wind speed and direction at 55 m a.g.l. from data for 2001.

- use the modelled wind farm wind speed as a basis for the wind speed prediction.

Using the NCEP/NCAR reanalysis as a mock 0-hour look ahead time forecast through 2001 and comparing with wind speed measurements at the wind farm site it is possible to assess the performance of the wind class look-up table approach.

Predictions using the NCEP/NCAR geostrophic wind at 0 m of the appropriate wind class directly as the farm wind speed give a mean error (ME) of -1.0 ms^{-1} and a mean absolute error (MAE) of 4.6 ms^{-1}. Predictions using the modelled winds at the wind farm of the appropriate wind class simulation give a mean error of -1.4 ms^{-1} and a mean absolute error of 3.8 ms^{-1}.

These errors were calculated before applying any model output statistics (MOS). It shows when using the KAMM modelling winds rather than the geostrophic winds, that although the bias becomes more negative, the mean absolute error becomes smaller, indicating that the spread of the error becomes smaller. The more negative bias is possibly due to the absence in the mesoscale modelling of the microscale speed-up effect.

Using MOS on the modelled winds at the wind farm gives a mean error of 0.3 ms^{-1} and a mean absolute error of 3.1 ms^{-1}. This brings the performance close to that of the GFS and MOS predictions. It should be remembered that the NCEP/NCAR reanalysis model uses a much lower resolution grid, approximately 2.5 x 2.5°, in contrast to the GFS forecast model grid, approximately 0.5 x 0.5°. It should also be remembered that the prediction period is not the same in the two cases.

The modelling study with the NCEP/NCAR reanalysis based wind classes and the idealized forcing study showed encouraging signs that the mesoscale modelling could capture

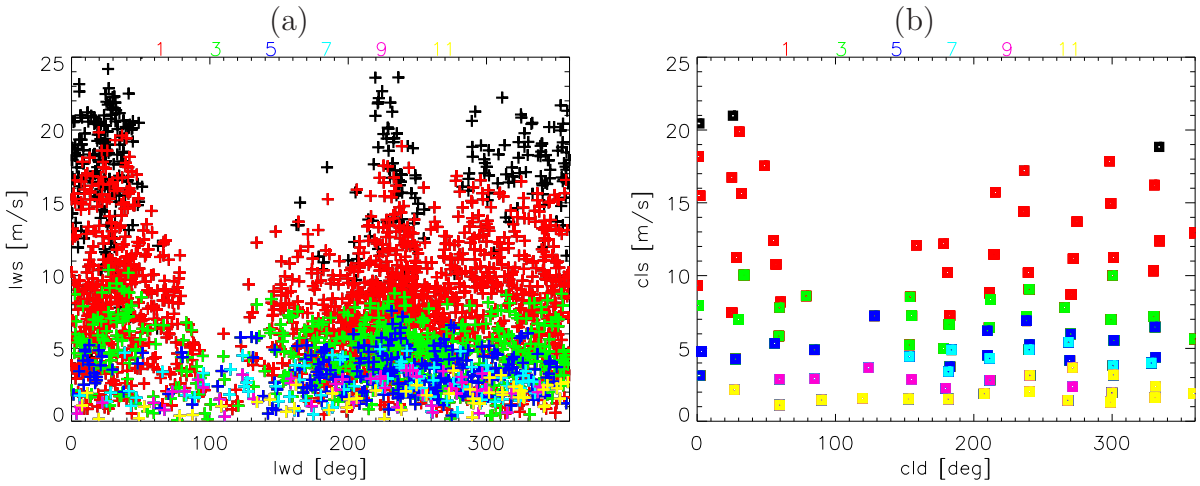

Figure 8: (a) The geostrophic wind and direction derived from GFS forecasts for the period 01/07/2004 - 31/05/2005 at a grid point close to the Alaiz wind farm. (b) The geostrophic wind and direction for the 103 wind classes that have been calculated to represent the data in (a). The colours of the plotted points indicate the values of $1/Fr^2$, the colour key is provide by the colour of the values above the plots.

the characteristics of the local wind flow around a wind farm site.

However the NCEP/NCAR reanalysis cannot provide a real forecast, therefore the next step was to use data from the GFS system. It is a good idea to use the same meteorological model to create the wind classes as is used to provide the data for the predictions. Therefore a new set of wind classes was created using the GFS data and a new set of KAMM simulations performed. The geostrophic wind speed and direction derived from the GFS data for the period 01/07/2004 - 31/05/2005 at the nearest grid point and the derived wind classes are shown in Fig. 8.

Without using MOS the GFS and KAMM look-up table predictions give a mean error of -0.66 ms^{-1} and a mean absolute error of 3.46 ms^{-1}, based on a forecast look-ahead time in the range 0 to 48 hours. Although the data period is not the same as for the NCEP/NCAR and KAMM look-up table prediction, it can be noted that there is is an improvement of mean error and mean absolute error of 51% and 9% respectively, even though it is a true forecast rather than a reanalysis. A lot of the improvement is probably due to the GFS providing a better description of the geostrophic wind in the region.

Using MOS on the GFS and KAMM look-up table predictions gives a mean error of -0.11 ms^{-1} and a mean absolute error of 2.60 ms^{-1}. This compares favourably with the predictions made using GFS and MOS alone, giving a mean absolute error of 2.98 ms^{-1} for Alaiz, as described in section 5.

8 Validation of modelling results with WRF

8.1 Validation of the region wind flow modelling around the Alaiz wind farm using WRF

The mesoscale simulations described and used so far in this report have been performed using the model KAMM. Within the Intelligent Prognosis project description the need to validate results has been stated. Within this work package validation has been carried out by comparing wind speed prediction with wind speed measurements at the Risø, Aliaz and Klim. The step in the validation process is to check model results from KAMM with a second mesoscale model. The second mesoscale model is the WRF model, which stands for the Weather Research and Forecasting model. There are in fact two versions of the model one called ARW (Advanced Research WRF) and NMM (Non-hydrostatic Mesoscale Model). The ARW version is used here because it features an option to use an initialization method rather like that used for KAMM. Skamarock et al. (2005) gives a detailed description of the WRF/ARW model.

As much as possible the same mesoscale simulation were performed using WRF as were performed using KAMM. Because the models are set up differently an exact replication of the model initialization is not possible. However some characteristics of the way WRF can be initialized are similar to KAMM. For this reason WRF made a good candidate for the validation studies.

The horizontal extent of the calculation domain used in WRF was the same as that used in KAMM, i.e. the 400 x 400 km domain using the same elevation (as shown in Fig. 3 and surface roughness for the lower boundary. So although the differing numerical handling of surface elevation (the two models use different vertical coordinate systems) and surface roughness (the models use different surface layer parameterizations), the values for surface input data for the domain are the exactly the same.

KAMM uses an implementation of a boundary condition at the top model the prevents reflection of gravity waves at the model upper boundary. This boundary condition is not implemented in the WRF model. Instead for the same purpose a damping layer is used at the top of the model. The damping layer for the Aliaz domain was from 12 to 15 km. In this region Rayleigh damping acts to restore the atmosphere to the initial state.

As in KAMM a stretched vertical coordinate was used, giving a finer vertical spacing of the model levels nearer the surface. Another important difference in the two models is the type of grid used. KAMM uses a Arakawa A-grid, where as WRF/ARW uses a Arakawa C-grid.

The way in which the forcing atmospheric profiles are set up is similar to that in KAMM. The profiles, also known as soundings, describe the change with height of geostrophic

wind speed, direction, potential temperature and specific humidity. Specific humidity, as well as surface moisture content, were set to zero, in order to replicate the dry atmosphere modelling of KAMM. The idealized input profiles were based on the output of the KAMM initialization routines. Because of the damping layer, the KAMM initialization profiles had to be extended to the higher model upper boundary of WRF.

This way of initializing WRF is a modificaton to the standard idealized configurations. A switch was set in the WRF configuration such that the Coriolis force was only calculated for the perturbation winds, i.e. winds deviating from the initial profile. This is equivalent to the KAMM configuration, in that the initial profile represents the large-scale geostrophic forcing.

Just as in the KAMM simulations, WRF simulations were performed using idealized sets of wind profiles representing different wind directions and different atmospheric stabilities; four different geostrophic wind speed profiles (5, 10, 15, 20 m/s) and three different stabilities, neutral, typical (near neutral) and stable.

Figure 9 summarizes the results from five sets of the idealized WRF simulations. The data is presented in the same way as in Fig. 4. The winds shown in Fig. 9 are for the four nearest grid points to the Alaiz wind farm at 3 hours of model time after initialization.

Qualitatively, the results from the idealized WRF simulations are very similar to the results from the idealized KAMM simulations. Comparing Fig. 4 and Fig. 9, it is seen that the WRF results give very similar wind direction concentration and wind speed enhancement effects. Similarly the wind direction concentration and wind speed enhancement effects are strongest for the low wind speed and stability cases. The dominant angles for the wind direction concentrations are 330 - 0° and 130 - 150°. This is also in very good agreement with the KAMM results.

Small differences between the results from the two models are found for the wind forcings that give weak wind speeds at the wind farm. In these cases the wind directions at the wind farm location may disagree by 10s of degrees, although the wind speed can be in reasonable agreement.

The levels of the wind speed enhancements is very similar between the two model results, shown by the length of the radial lines relative to the cirle in each plot.

8.2 Validation of the wind class system and a look-up table approach to short-term wind speed prediction using WRF

WRF has beed used to make a look-up table prediction system just as KAMM was used in subsection 7.2. Comparison of the results of the error analysis for the KAMM and WRF based look-up tables gives a quantitative comparison between the two model.

The WRF initialization profiles were the same as those used with KAMM based on GFS data for the period 01/07/2004 - 31/05/2005 at the nearest GFS grid point. The geostrophic wind speed and wind direction and the 103 derived wind classes are shown in Fig. 8(b).

The mesoscale models' wind speed and direction at 50 m a.g.l. for each of the 103 wind classes at the wind farm location is shown in Fig. 10(a) and (b), for KAMM and WRF respectively. As in the the idealized profile simulations, the wind direction concentration effects of the regional terrain are evident in both models. It can be seen however that simulation wind speed and direction from each model differ for each wind class because the details of Fig. 10(a) and (b) differ not insignaficantly. The main differences are that whereas KAMM produces winds in the ranges 0 - 130° and 0-5ms^{-1}, WRF does not produces winds within these ranges. Measurements from Alaiz suggest that indeed winds within these ranges are very rare (see Fig. 7, although these data are for 2001). On the other hand the KAMM results produce no winds in the ranges 30 - 100° and 200 - 300° and greater than 10 ms^{-1}, whereas WRF produces 4 wind classes within these ranges. Measurements suggest the also that winds within these ranges is very rare.

Table 3 summaries the performance of the KAMM and WRF look-up table prediction systems. First, looking at the mean error and mean absolute error for the two systems without using MOS, it can be seen that the WRF look-up table system does not perform as well as the KAMM look-up table system. However it does still perform better than using the wind class geostropic winds alone which gives a mean absolute error is 4.19 ms^{-1}. After MOS the performance of the two models' look-up tables is rather similar. It should be repeated that this performance is better than using GFS surface wind data (U_{30-0}) for the wind farm location and MOS.

	no MOS		with MOS	
Model	ME	MAE	ME	MAE
KAMM	-0.66	3.46	-0.11	2.60
WRF	-1.18	3.78	-0.15	2.65

Table 3: Mean error (ME) and mean absolute error (MAE) in m/s for predictions made using KAMM and WRF look-up tables without MOS and with MOS.

9 Stability preprocessing for WPPT

In this section a concept for integrating a stability measure into the Wind Power Prediction Tool (WPPT) developed by IMM/DTU is described.

Figure 11(a) shows the flow of information from the numerical weather prediction model and the wind farm into WPPT. Currently the wind speed and direction come directly into

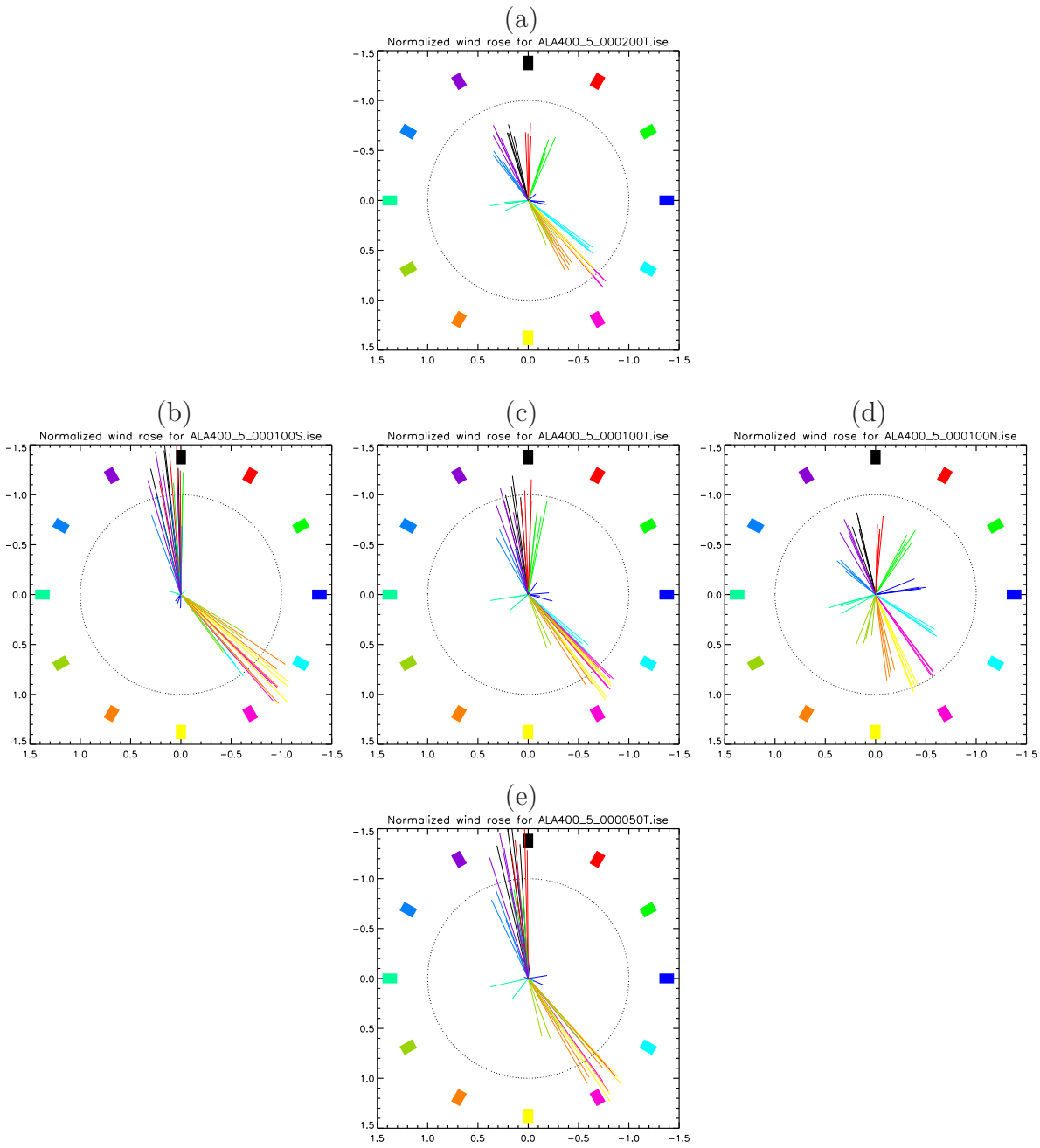

Figure 9: Diagrams showing the mesoscale effects on the geostrophic wind forcings for 5 sets of WRF simulation using different wind speed and thermal stratifications, (a) 20 ms^{-1} and typical stability, (b) 10 ms^{-1} and stable conditions, (c) 10 ms^{-1} and typical stability, (d) 10 ms^{-1} and neutral conditions, (e) 5 ms^{-1} and typical stability. Each set is made up of 12 simulations using different wind direction indicated by colour. Please refer to the main text for an explanation of the figures.

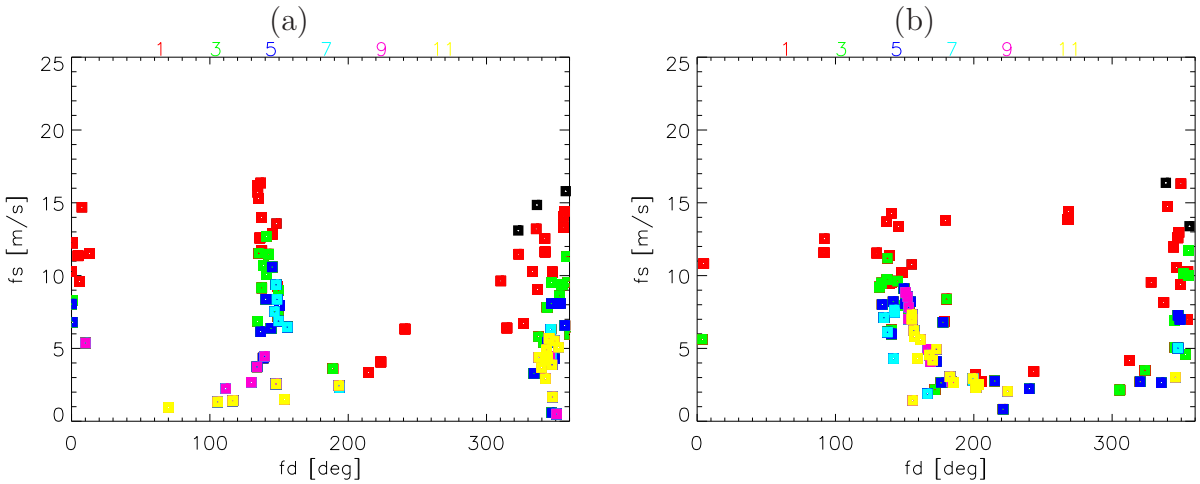

Figure 10: (a) The KAMM modelled wind speed and direction at 50 m a.g.l. at the wind farm site resulting from the simulations using the 103 GFS derived wind classes shown in Fig. 8(b). (b) The WRF modelled wind speed and direction at 50 m a.g.l. at the wind farm site resulting from the same GFS derived wind classes.

WPPT from the weather forecast provider and measurement of wind power is fed back into WPPT to allow for recursive adjustment of the farm power curve within WPPT.

Instead of making drastic changes to WPPT in order to include the stability parameter, by for instance adding an extra dimension to the farm power curve model, a preprocessor concept is employed. This saves considerably on any reprogramming within WPPT at this preliminary stage when the benefits to WPPT performance due to the inclusion of a stability measure are not well known. The extra process is shown in Fig. 11(b). The NWP provided data, including the appropriate stability measure, is feed into the preprocessor. The preprocessor applies the linear regression using coefficients determined from an earlier training period. The output of the preprocessor is simply the stability corrected wind speed and direction ready for input into WPPT. WPPT operates in just the same way as it did before the preprocessor was added, i.e. exactly the same kind of input and output operations are performed.

A more advanced version of the preprocessor is shown in 11(c). In this version the measured wind speed and measured farm power are fed into the preprocessor so that the linear regression coefficients can be updated recursively. The recursive features of WPPT bring many advantages to the system, such as accommodation of seasonal variations, dirtying of turbine blades, changes to the operation of the NWP system, etc. Thus a recursive adjustment of a stability correction is considered advantageous.

In order to test this concept, off-line trials of the preprocessor will be carried out using the Alaiz wind farm as the case study. The trials will use the following input time series for WPPT:

- Control 1
  U_{10} and D_{10} from GFS.
- Control 2
  U_{30-0} and D_{30-0} from GFS.
- Control 3
  U_{hub} and D_{hub}, given by an interpolation of U_{10} and U_{10} based on log profile.
- Experiment 1
  U^1_{prep} and D^1_{prep}, based on U_{10}, D_{10}, and deep profile N^2.
- Experiment 2
  U^2_{prep} and D^2_{prep}, based on U_{30-0}, D_{30-0}, and deep profile N^2.

The performance of WPPT using these different input time series will be compared. Any improvement gained by the experimental time series over the control 3 time series will indicate that there is a local effect of the stability begin captured, rather than simply better information being gained by having defining the wind speed profile as it is in the NWP model.

10 Conclusions

An investigation into the use of various stability measures as part of a simple wind speed prediction method has been been carried out. The method is based on a linear regression of NWP wind speed forecasts and NWP stability forecasts. The investigation used three sites. At two of the sites improvements were seen when using a stability measure as part of the linear regression.

For the Risø mast the improvements, measured in terms of mean absolute error, were small (<1%) for predictions based on U_{30-0}, but somewhat larger (2-5%) for predictions based on U_{10}. The improvement came about through use of the shallow profile stability measures, which are based on meteorological quantities in the lowest 1 km or so of the atmosphere. However the performance using U_{10} whatever the stability parameter never beat the prediction performance using U_{30-0} alone.

For the Alaiz mast the improvements were more dramatic. The wind speed predictions improved most when the deep profile Brunt-Väisälä frequency, N^2, was used for the stability parameter, calculated using meteorological quantities at heights between approximately 0 - 3000 m. The prediction based on U_{30-0} improved by 17% and the prediction based on U_{10} improved by 20%. In summary the prediction based on U_{30-0} and N^2 gave the best performance.

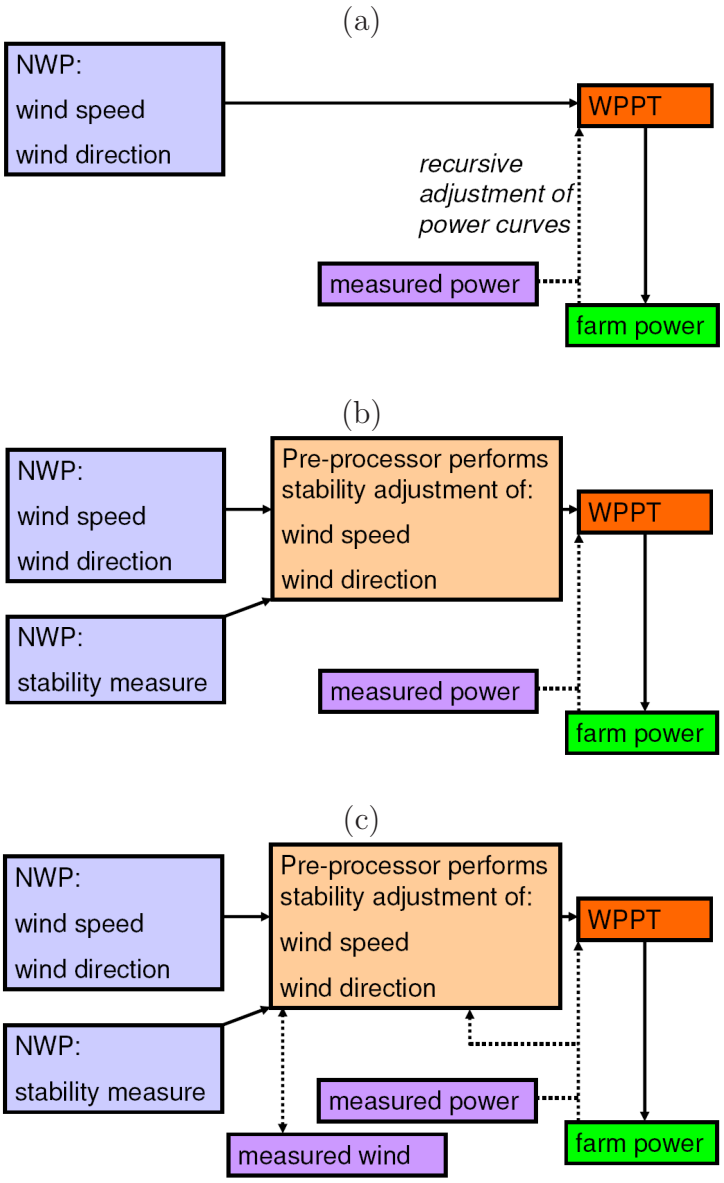

Figure 11: Schematic diagrams showing the conceptual development of the WPPT pre-processor.

Mesoscale modelling in a 400 x 400 km region centred on the Alaiz wind farm was carried out using KAMM. First an idealized study was performed using 72 simple velocity profiles and 3 characteristic temperature profiles to force the model. The profiles were determined up to a height of 5.5 km in the atmosphere. These idealized model simulations demonstrated the direction concentrating and speed-up effects of the topography around the wind farm, and showed that these effects are sensitive to the Froude number.

The wind classification system, from the numerical wind atlas methodology developed at Risø, was used to create 108 wind and temperature profiles representing the large scale forcings that occurred in the region in the year 2001 based on NCEP/NCAR reanalysis data. Simulations using these wind classes demonstrated that the modelled winds could capture the characteristics of the measured distribution of the wind speed and direction at the wind farm for the same year.

A look-up table was created that associated the large scale wind classes with the modelled winds at the wind farm site. A mock prediction system was constructed using the NCEP/NCAR reanalysis data as a 0 hour leadtime forecast and the look-up table. The mean absolute error for this prediction system after MOS was similar to that of the GFS predictions after MOS.

The mean absolute error of the KAMM look-up table approach was reduced when using GFS data to determine the wind classes and provide prognosis of the wind and temperature profiles. In that case the mean absolute error is 13% smaller than the mean absolute error using GFS and MOS alone.

Deep profile stability information is an integral part of the wind class system. Within a small range of wind speeds and directions more than one wind class will be generated, in order to capture the various stability conditions that may occur. Figure 6(b) shows that for a given wind speed and direction there are often pairs of wind classes, each representing a less stable or more stable situation respectively.

Some experimentation was carried out with the wind class generating programs to see the impact of changing the emphasis of the stability. For example, is performance improved when allowing three stability situations within a small range of wind speeds and directions, instead of two? This question is still not conclusively answered.

The use of WRF, in place of KAMM, has validated that mesoscale modelling can be used to evaluate properties of the region flow around a wind farm site. These properties can be applied in the form of a look-up table to adjust geostrophic wind and temperature profiles from numerical weather prediction model forecast to give winds at the wind farm site.

The idealized simulations using WRF suggest a strong qualatitive agreement with the simulations using KAMM. The comparison of the look-up table prediction systems using KAMM and WRF suggest a slightly better perforance by KAMM. However the experi-

ence in this kind of application of WRF is smaller than that with KAMM. With some adjustments to the WRF configuration a similar performance or better could be expected.

The frame work for the integration of the stability based linear regression method into the wind power prediction system WPPT is given. This method in the form of a preprocessor gives a straight forward way to test whether the improved wind speed predictions for the Aliaz wind farm can in turn can be used to provide improved wind power predictions. If the first trials show encouraging results the method can be made more advanced. Features such as recursive adjustment of the regression coefficients are proposed.

11 Acknowledgments

The Danish PSO fund is greatly acknowledged for sponsoring this study as part of Intelligent Prognosis for Wind Energy project (FU4101). The first experiments using mesoscale modelling for the Aliaz wind farm were conducted under the EU funded ANEMOS project (ENK5-CT-2002-00665). The Intelligent Prognosis project has benefitted from the experience gained in that earlier project. Ignacio Martí of CENER, Spain, is thanked for his assistance in providing the Alaiz wind farm data and the GFS forecast data used in section 5. Karlsruhe University/Research Center Karlsruhe is acknowledge for permission to use KAMM. NCEP is acknowledged for making available the data from the GFS forecast system. As part of the collaborative partnerships developing the mesoscale model WRF the following institutions in the U.S.A. are acknowledged the National Center for Atmospheric Research (NCAR), the National Oceanic and Atmospheric Administration (the National Centers for Environmental Prediction (NCEP) and the Forecast Systems Laboratory (FSL), the Air Force Weather Agency (AFWA), the Naval Research Laboratory, Oklahoma University, and the Federal Aviation Administration (FAA).

References

Adrian, G. and Fiedler, F. (1991). Simulations of unstationary wind and temperature fields over complex terrrain and comparion with observations. *Beitr. Phy. Atmosph.*, 64:27–48.

Dyer, A. J. (1974). A review of flux-profile relationships. *Boundary-Layer Meteorology*, 7:363–372.

Frank, H. P. and Landberg, L. (1997). Modelling the wind climate of ireland. *Boundary-Layer Meteorology*, 85:359–378.

Frey-Buness, F., Heimann, D., and Sausen, R. (1995). A statistical-dynamical downscaling procedure for global climate simulations. *Theor. Appl. Climatol.*, 50:117–131.

Giebel, G., Badger, J., Louka, P., Kallos, G., Perez, I. M., Lac, C., Palomares, A.-M., and Descombes, G. (2005). Short-term forecasting using advanced physical modelling: The

results of the anemos project: Results from mesoscale, microscale and cfd modelling. *http://anemos.cma.fr/download/publications/pub_2006_paper_EWEC06_WP4physical.pdf*.

Hogström, U. (1988). Non-dimensional wind and temperature profiles in the atmospheric surface layer: A re-evaluation. *Boundary-Layer Meteorology*, 42:55–78.

Jensen, N. O., Petersen, E. L., and Troen, I. (1984). *Extrapolation of mean wind statistics with special regard to wind energy applications*. World Meteorological Organization.

Kaimal, J. C. and Finnigan, J. J. (1994). *Atmospheric Boundary Layer Flows*. Oxford University Press.

Skamarock, W. C., Klemp, J. B., Dudhia, J., Gill, D. O., Barker, D. M., Wang, W., and Powers, J. G. (2005). A description of the advanced research wrf version 2. *NCAR Technical Note NCAR TN 226468+STR*.

Risø's research is aimed at solving concrete problems in the society.

Research targets are set through continuous dialogue with business, the political system and researchers.

The effects of our research are sustainable energy supply and new technology for the health sector.